A model of solar total and spectral irradiance variations

M. Fligge[1]**, S.K. Solanki**[1]**, Y.C. Unruh**[2]**, C. Fröhlich**[3]**, and Ch. Wehrli**[3]

[1] Institute of Astronomy, ETH-Zentrum, CH-8092 Zürich, Switzerland
[2] Institute for Astronomy, University of Vienna, Türkenschanzstrasse 17, A-1180 Wien, Austria
[3] Physikalisch-Meteorologisches Observatorium Davos, World Radiation Center, CH-7260 Davos Dorf, Switzerland

Abstract. We model solar spectral irradiance variations under the assumption that they are produced by sunspots and faculae alone. The model is based on three components, i.e. quiet Sun, assumed to be temporally invariant, sunspots and faculae whose temporal variations are mimicked using time series of sunspot areas and Mg II core-to-wing ratios. The detailed flux spectrum for each component is employed.

The results are compared to spectral irradiance measurements at 402 nm, 500 nm and 862 nm obtained between February 22 and December 31, 1996 by the three-channel sunphotometers (SPM) which are part of the VIRGO package onboard SOHO. Our model shows a good correlation with the measured variations of the three colour channels and of the total irradiance. Since it also successfully reproduces changes in the UV spectral irradiance, irradiance variations and observed variations of the faculae-to-spots filling factor ratio since 1978, our model supports earlier suggestions that a large part of the solar irradiance variations is caused by magnetic fields at the solar surface.

Finally, we use the model to test whether the difference between the magnitude of solar and stellar brightness variations reported by Lockwood et al. (1992) is due to the particular filters they use for their stellar observations. Our results suggest that this effect can explain only a small part of the discrepancy.

Key words: Sun: activity – Sun: faculae, plages – Sun: magnetic fields – sunspots

1. Introduction

Since the first space-borne measurements of solar irradiance in the late seventies, the Sun has now been constantly monitored for almost two complete activity cycles with a precision high enough to detect even variations of the order of 0.01% (Willson & Hudson 1988, Fröhlich & Lean 1998). These observations revealed a remarkably inconstant Sun whose brightness varies in phase with the solar activity cycle. The total solar irradiance, dominated by visual and IR radiation, differs by approximately 0.1

The variations are known to have a strong wavelength dependence (Lean 1991, Pap 1992, Rottman et al. 1994, Lean et

al. 1997). The UV spectrum at wavelengths well below 300 nm exhibits variations that are orders of magnitude larger than those in the visible and IR (see Fig. 10). While contributing less than 1% to the total irradiance value the UV radiation contributes approximately 14% to the *variation* of the total irradiance (Lean 1991, Solanki & Unruh 1998; henceforth referred to as SU98).

The strong wavelength dependence of solar spectral irradiance variations plays an important role in the way the Sun influences the Earth's climate system. While visual and near IR radiation is only moderately attenuated by the Earth's atmosphere, solar UV radiation below 300 nm is almost completely absorbed in the upper atmosphere and stratosphere where it significantly alters the chemical composition and dynamical evolution of those layers and controls the amount of variability of the ozone concentration (Brasseur & Solomon 1984, Rees 1989, Lean 1991, Haigh 1994, 1996).

The spectral dependence of the solar UV irradiance variations between solar activity maximum and minimum was successfully modelled by SU98 based on a simple three-component model. It is important to test this promising model further in order to reveal possible shortcomings and point the way towards further improvements. Since the dominant part of the irradiance variations arises in this wavelength range particular emphasis should be placed on it.

Until recently, the spectral dependence of the irradiance in the visible was unknown. With the successful launch of SOHO (Solar and Heliospheric Observatory) at the end of 1995 we now have simultaneous measurements of total as well as spectral irradiance variations at three different wavelengths. Such observations are carried out every minute by the VIRGO (Variability of Irradiance and Gravity Oscillations) experiment onboard SOHO (Fröhlich et al. 1995, 1997).

In the present paper we use the VIRGO and the composite of total solar irradiance (TSI) measurements constructed by Fröhlich & Lean (1998) in addition to the previously used UV data and relative filling factors to set tighter constraints on the model and to reveal its limits.

Details about the observations and data sets are given in Sect. 2. In Sect. 3 we briefly describe the model, the employed spectra and the reconstruction procedure of temporal variations. In Sect. 4 we model the VIRGO measurements and discuss the results. We use our model to reconstruct solar irradiance over
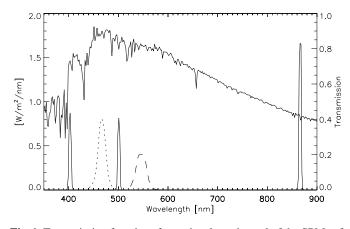

Send offprint requests to: M. Fligge

Fig. 1. Transmission functions for each colour channel of the SPMs of VIRGO (right-hand scale). The functions are centered around 862 nm (red channel), 500 nm (green channel) and 402 nm (blue channel) with a bandwidth of 5 nm each. Also plotted are the two Strömgren filterbands b and y (dotted and dashed lines, respectively) centered around 472 nm and 551 nm (for stellar observations). The left-hand scale refers to the modelled flux of the Sun.

nearly two complete solar cycles in Sect. 5, in which we also compare our findings to the composite TSI and to observations of the faculae-to-spots filling factor ratio. We test our model against UV irradiance observations obtained over the solar cycle in Sect. 6. We then use the reconstructed spectral irradiance to scale solar brightness variations to stellar observations and discuss our results in the context of the findings of Lockwood et al. (1992) in Sect. 7. Finally, in Sect. 8 conclusions are presented.

2. Irradiance measurements and the facular and sunspot proxies employed

The sunphotometers (SPM) within VIRGO measure spectral irradiance variations in three wavelength ranges centered at 402 nm (blue channel), 500 nm (green channel) and 862 nm (red channel) with a bandwidth of 5 nm each. The transmission functions of the three channels are plotted in Fig. 1 (solid; see also Fig. 7). The two Strömgren filterbands b (dashed) and y (dotted) used for stellar brightness measurements are plotted as well. We shall refer to them in Sect. 7. Also shown is the modelled flux spectrum of the Sun. In addition to the spectral irradiance measurements, VIRGO also records total irradiance using its active-cavity radiometers. Details about the instruments and observations are given in Fröhlich et al. (1995, 1997). All four sets of irradiance measurements are plotted in panels a–d of Fig. 2.

We are currently in a phase of low solar activity so that the irradiance measurements show only minor variations. Nevertheless, enhanced facular emission as well as a few dips caused by the passage of sunspots across the solar disk are clearly recognizable (see, e.g., the dips around the days $\sim$200 and $\sim$330 in Fig. 2a). We choose the time-period between February 22, 1996 (day 53) and the end of the year for all further investigations. This interval also includes the rather large sunspot groups (NOAO 7997 and 7999) in November of that year.

To investigate solar irradiance on time scales of the solar cycle we use the composite TSI of Fröhlich & Lean (1998). It is based on inter-calibrated time series of several space-borne irradiance experiments and provides a consistent record of total solar irradiance measurements over the last 18 years, i.e. almost two complete solar cycles.

The temporal variations of sunspots and faculae are mimicked using time series of sunspot areas $A_s(t)$ and Mg II core-to-wing ratio $R_{\mathrm{Mg}}(t)$, respectively. The two proxies describe the temporal variation of the spot and facular contributions, respectively. The sunspot areas A_s are measured almost daily in parts per million. They enter in a very direct manner into the model. They are taken from the NGDC (National Geophysical Data Center) database. Fig. 2f shows measurements of A_s for the time period of VIRGO measurements.

R_{Mg} has proved to be a good proxy of enhanced facular (and network) emission brightening (Heath & Schlesinger 1986, Lean 1988) due to its high correlation to irradiance residuals (i.e. total solar irradiance measurements corrected for sunspot dimming) and other proxies of solar chromospheric variability (Donnelly et al. 1994). We use the records of the Solar Ultraviolet Spectral Irradiance Monitor (SUSIM) onboard the Upper Atmospheric Research Satellite (UARS) for the time period of the VIRGO measurements. No single dataset of Mg II core-to-wing ratio measurements covers the whole time period of the composite TSI measurements. We therefore construct a consistent record by combining measurements of the Solar Backscatter Ultraviolet (SBUV) experiment onboard NIMBUS-7, SBUV/2 onboard NOAA-9 (both normalized to SUSIM) and of SUSIM. All facular proxies are available from the NGDC.

3. The 3-component model of solar irradiance

3.1. Flux spectra

The solar model we use is based on the assumption that irradiance variations are caused by magnetic features alone. It was originally proposed by SU98 and uses three components, namely quiet Sun, sunspots and faculae, to model solar irradiance. In its current form the model neglects the angular dependence of the radiance of magnetic features. Hence contributions to relative irradiance variations are described using flux values (SU98).

The quiet Sun model, F_{qs}, corresponds to the non-gray radiative equilibrium model of Kurucz (1991) with an effective temperature of T_{eff}=5777 K. It is assumed to be temporally invariant. For the reconstructions we employ the flux spectrum produced by this model.

Since the temperature structure of umbrae (Severino et al. 1994) and penumbrae is close to that expected from radiative equilibrium (Del Toro Iniesta et al. 1994), the contribution of sunspots F_{s} is modelled using a Kurucz flux spectrum of T_{eff}=5150 K. This temperature is 100 K lower than that employed by SU98. It still corresponds to a ratio of umbral to penumbral area of approximately 1:3 and results in a somewhat better fit to the data. Employing the flux spectra of the umbra
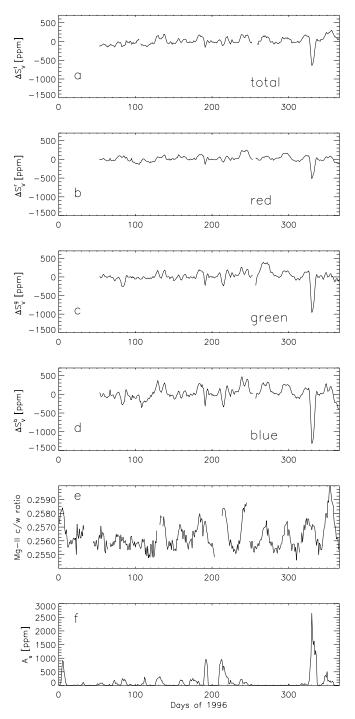
Fig. 2. Time series of total (**a**) and spectral relative irradiance variations (**b-d**) and of the two proxies R_{Mg} (Mg II core-to-wing ratios, (**e**) and A_s (sunspot areas, **f**) used to mimic temporal behavior of faculae and sunspots. Total and spectral irradiance values are given as relative deviations from the mean (ΔS, see Eq. 5) in parts per million. The total irradiance measurements are obtained by the VIRGO radiometers and the spectral irradiances are measured by the SPMs of VIRGO. The Mg II core-to-wing ratio is recorded by the Solar Ultraviolet Spectral Irradiance Monitor (SUSIM) and the sunspot areas were provided by the National Geophysical Data Center (NGDC), respectively.
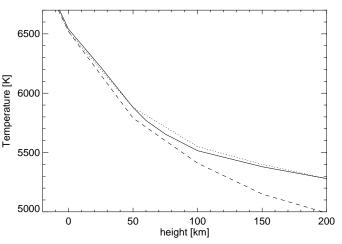

Fig. 3. Comparison between the facular model of Fontenla et al. (1993) as modified by Solanki & Unruh (1998, FAL-P1; dotted) and the version used in this study (FAL-P2, solid). Also shown is a quiet Sun model with effective temperature T_{eff}=5770 K (dashed).

and penumbra separately (while keeping the ratio of umbral to penumbra area fixed) does not change the results significantly. We therefore do not consider this extension to the model further.

Finally, the facular contribution, i.e. the third component, is based on the facular model atmosphere of Fontenla et al. (1993; FAL-P). SU98 had to fine tune this model in order to match the UV spectral irradiance variations. The additional constraints imposed by requiring that both the visible spectral irradiance variations observed by VIRGO and the UV variations are reproduced require further minute modifications to the model.

The temperature stratification of the model that reproduces the whole set of observations best is plotted in Fig. 3 (FAL-P2, solid) together with the model of Fontenla et al. (1993) as modified by SU98 (dotted; FAL-P1) and a quiet Sun model, FAL-C (dashed), with an effective temperature of T_{eff}=5770 K. Obviously the FAL-P2 temperature stratification deviates only slightly from that of FAL-P1. The temperature of the faculae between 0 km and 50 km has been increased slightly in order to improve the fit of the reconstructed time series to the data measured by VIRGO, whose colour channels are sensitive to radiation formed at these heights (see Fig. 7). To compensate for the resulting brightness enhancement and to keep the variability over the solar cycle at the 0.1% level the temperature between 50 km and 200 km (where most of the UV irradiance variations are formed) has been correspondingly decreased.

The flux spectrum of the facular component is calculated following SU98, i.e. using the Planck function to convert the spectrum into temperature values and assuming that the radiation in faculae is formed at the same height as in the quiet Sun model. As in that paper the small-scale structure of faculae is neglected.

Table 1. Contrasts, C, for the used spot and facular models at the four spectral ranges of VIRGO.

	Total	Red	Green	Blue
Spots	−0.3566	−0.3186	−0.4811	−0.5908
FAL-P2	0.0597	0.0352	0.0723	0.0988

We list in Table 1 the contrasts, C, of the spot model with T_{eff}=5150 K and the facular model, FAL-P2, for each of the irradiance channels of VIRGO. The contrasts are defined by

$$C_\Lambda = \frac{\int_\Lambda F(\lambda)\, d\lambda}{\int_\Lambda F_{\text{qs}}(\lambda)\, d\lambda} - 1, \tag{1}$$

where the integration runs over Λ, the wavelength range considered (i.e., the total, red, green or blue colour channel). F stands for the flux spectra of the spots or faculae, respectively, and F_{qs} for the quiet Sun. The sunspot contrast (about 0.36 for the total) is somewhat larger than values usually used to model sunspots using the photometric sunspot index (PSI; Hudson et al. 1982, Fröhlich et al. 1994, Steinegger et al. 1990). This choice is driven mainly by the need to reproduce the large dips due to sunspot blocking during activity maximum. A slight increase of T_{eff} of the sunspot model basically leads to less deep dips, while having little effect on the rest of the analysis.

To calculate the solar flux $F_{\text{tot}}(\lambda)$ as a measure for the irradiance at a wavelength λ we combine the fluxes from the three model components as follows:

$$\begin{aligned} F_{\text{tot}}(\lambda, t) = (1 - \alpha_{\text{s}}(t) - \alpha_{\text{f}}(t)) \cdot F_{\text{qs}}(\lambda) \\ + \alpha_{\text{s}}(t) \cdot F_{\text{s}}(\lambda) \\ + \alpha_{\text{f}}(t) \cdot F_{\text{f}}(\lambda), \end{aligned} \tag{2}$$

where F_{s} is the flux of the spots, F_{f} stands for the flux of the faculae and α_{s} and α_{f} represent spot and facular filling factors, respectively. In general α_{s} and α_{f} are time dependent (the fraction of the solar surface covered by sunspots and faculae varies strongly), but in our model F_{qs}, F_{s} and F_{f} are not. We hence assume that any changes in solar irradiance are due to magnetic features (including magnetic elements in the quiet Sun). Also, we assume that all sunspots and all faculae have the same spectra and contrasts. Whereas the former is open to debate, the latter is certainly not correct, but is at present unavoidable due to lack of better data. Following (2) we obtain fluxes at a set of wavelengths covering a wavelength range of 174 nm to 100 μm. The individual wavelength bins increase from 1 nm at 174 nm to 20 μm at 100 μm as dictated by Kurucz's flux spectra.

3.2. Reconstruction of temporal variations

In order to reproduce the time dependence of total and spectral irradiance variations we keep F_{qs}, F_{s} and F_{f} temporally invariant, while allowing α_{s} and α_{f} to vary with time. Whereas $F_{\text{qs}}(\lambda)$, $F_{\text{s}}(\lambda)$ and $F_{\text{f}}(\lambda)$ are calculated as in Sect. 3.1, we need

additional observed parameters to serve as proxies for $\alpha_{\text{s}}(t)$ and $\alpha_{\text{f}}(t)$ (see Sect. 2).

We define the temporal variations of the spot and facular filling factors by

$$\begin{aligned} \alpha_{\text{s}}(t) &= a_{\text{s}} \cdot A_s(t) \\ \alpha_{\text{f}}(t) &= a_{\text{f}} \cdot R_{\text{Mg}}(t) \end{aligned} \tag{3}$$

where the parameters a_{s} and a_{f} determine the scaling factors between the proxies (A_s and R_{Mg}) and their corresponding filling factors. After combining Eqs. (2) and (3) we get $F_{\text{tot}}(\lambda, t)$, i.e. the solar flux spectrum as a function of time. Note that since we use flux spectra to calculate solar irradiance A_s is more compatible with our method of modelling than PSI, due to the inclusion of limb darkening in the latter.

The quality of the reconstruction of the time-dependent irradiance variations is mainly determined by the quality of the proxies used. Likewise, the standard deviation (RMS) of the time series of the reconstructed spectral irradiance variations are strongly influenced by the variability of the proxies. The RMS is therefore a simple measure of the mean irradiance variability over a given time span. However, the influence of the proxies on the goodness of the reconstructed irradiance variations relative to each other, i.e. the ratio between the different colour channels, is much smaller. This is because a poorly determined facular proxy to first order affects all colour channels equally (at least as long as the relation between the two proxies remains stable over the considered period of time).

In the following, when comparing the model with the observations, we need to distinguish clearly between the spectral irradiance variations predicted by the model, which is mainly determined by $F_{\text{s}}(\lambda)$ and $F_{\text{f}}(\lambda)$, i.e. finally by the spot and facular temperature stratifications, and the temporal variations, which are described by $\alpha_{\text{s}}(t)$ and $\alpha_{\text{f}}(t)$.

Before comparison with the observations, the flux spectrum must in general be further treated. The specifics of this treatment (e.g. integration over a limited wavelength range) depend on the particular data set we are comparing it with. This step will therefore be described separately in each of the following three sections in which we now test this model (and constrain its free parameters) using VIRGO spectral and total irradiance (Sect. 4), composite TSI (Sect. 5) and UV spectral irradiance observations (Sect. 6). We stress that although the comparisons with the different data sets are discussed separately, the fits were made in conjunction with each other and care was taken to ensure that the choices of free parameters used to reproduce the various data sets are consistent with each other.

4. Modelling VIRGO measurements

The values predicted by the model for each VIRGO channel c, i.e. $S^c(t)$, where c stands for either the t (total), r (red), g (green) or b (blue) channel, respectively, are calculated according to

$$S^c(t) = \int F_{\text{tot}}(\lambda, t) \cdot K^c(\lambda)\, d\lambda, \tag{4}$$

where $K^c(\lambda)$ is the transmission function of channel c (Figs. 1 and 7). We set $K^c(\lambda) \equiv 1$ for calculations of the total irradiance.

We then calculate relative variations in channel c according to

$$\Delta S^c(t) = \frac{S^c(t) - \langle S^c(t) \rangle_t}{\langle S^c(t) \rangle_t} \qquad (5)$$

where $\langle S^c(t) \rangle_t$ denotes the mean value of $S^c(t)$ averaged over the period of time considered.

From Eqs. (4) and (5) we can see that $\Delta S^c(t)$ does not change if $K^c(\lambda)$ is multiplied by a constant factor. In addition, the total reconstructed flux $F_{\text{tot}}(\lambda, t)$ varies only slightly over the wavelengths determined by $K^c(\lambda)$. This is partly due to the narrow bandwidth of the sunphotometers and partly due to the limited resolution of the employed flux models which do not resolve the various spectral lines present in the bandpass, especially in the blue part of the spectrum. Both effects cause the reconstructed *relative* irradiance variations to be rather insensitive to the exact shape of the transmission function of each channel. Nevertheless we use the measured K^c of the VIRGO sunphotometers for the reconstructions.

Once the flux models for the three components are fixed, only a_s and a_f have to be determined. This can be done, e.g., by least-square fitting of $\Delta S^c(t)$ to the VIRGO time series, $\Delta S_V^c(t)$. However, this may not be appropriate since many features seen in $\Delta S_V^c(t)$ have only a low statistical significance due to the current low level of solar activity. We therefore determine a_s and a_f using two different criteria based on the RMS values of the time series over the whole period. The proposed criteria are sensitive to opposite modeling aspects. The first criterium is minimization of the function

$$\Gamma_1 = \sqrt{\sum_c \left(1 - \frac{\sigma(\Delta S_V^c(t))}{\sigma(\Delta S^c(t))} \right)^2}, \quad c = t, r, g, b, \qquad (6)$$

which is significantly influenced by the quality and completeness of the used proxies since the absolute RMS values of $\Delta S_V^c(t)$ and $\Delta S^c(t)$ must be the same to minimize Γ_1. Secondly, we determine a_s and a_f in such a way that the function

$$\Gamma_2 = \sqrt{\sum_c \left(\frac{\sigma(\Delta S_V^t(t))}{\sigma(\Delta S_V^c(t))} - \frac{\sigma(\Delta S^t(t))}{\sigma(\Delta S^c(t))} \right)^2}, \quad c = r, g, b, \quad (7)$$

is minimized, i.e. we optimize the ratios between the RMS values of different channels with respect to the ratios found by VIRGO. Therefore Γ_2 is mainly sensitive to the employed model temperature stratifications, i.e. the used flux spectra for each of the three components, and less to the quality of the employed proxies. A priori, Γ_1 and Γ_2 are not expected to give the same values for a_s and a_f. The overall best representation of the data is given by the (a_s, a_f) pair which minimizes both Γ_1 and Γ_2.

In the following we first discuss the results of a reconstruction based on the solar model described in Sect. 3 using facular model FAL-P2. The results of a somewhat different model using a modified FAL-C to describe faculae are discussed at the end of this section.
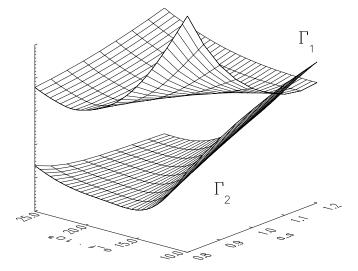

Fig. 4. Surface plots Γ_1 and Γ_2 for a fit of the model described in Sect. 3 to the VIRGO data. The common minimum lies around $(a_s, a_f) \approx (0.97, 18.0 \cdot 10^5)$. The value of $a_s \approx 1$ suggests an appropriate effective temperature for the sunspot model.

The two functions Γ_1 and Γ_2 are plotted in Fig. 4 over the parameter ranges $0.8 \leq a_s \leq 1.2$ and $10 \cdot 10^5 \leq a_f \leq 25 \cdot 10^5$. The upper surface plot shows Γ_1 while Γ_2 is represented by the lower surface plot. Both functions show no unique minimum. A change in a_s can be compensated by a corresponding change in a_f. The "valleys" of minimum Γ_1 and Γ_2 do not lie parallel to each other in the (a_s, a_f) plane, however. The point at which the minima of these two functions intersect is expected to be the best (a_s, a_f) pair to represent the data. The points of intersection lie at $a_s = 0.97 \pm 0.07$ and $a_f = (18.0 \pm 1.3) \cdot 10^5$. The error estimates are based on observational uncertainties in A_s and R_{Mg}.

The fact that the minimum is found to lie around $a_s \approx 1$ means that the effective temperature $T_{\text{eff}} = 5150$ K chosen to represent the sunspots is appropriate, although a somewhat higher temperature is also allowed.

In Fig. 5 we present a reconstruction of total (a) and spectral (b–d) relative irradiance variations as measured by VIRGO for the time between February 22, 1996 and December 31, 1996. We plot both observed (dotted) and reconstructed (solid) data. The (a_s, a_f) values used (0.97, 18.0) corresponds to a faculae-to-spots filling factor ratio of ≈ 20, when averaged over the modelled period. This filling factor ratio is in good agreement with directly observed ratios at solar minimum (Chapman et al. 1997).

Table 2 compares the four channels numerically. Given are the absolute standard deviations for each channel as well as the ratios between different channels for both, the observed and reconstructed time series, respectively. Deviations in percentage with respect to the values obtained for VIRGO are given in parentheses. The values of a_s and a_f have been chosen such that the errors of the total, red and green channels are about the same. It is possible, by changing a_s and a_f slightly, to improve the reconstruction for the total, red and green channels and to push
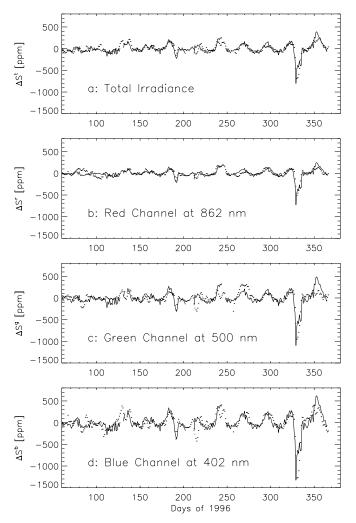
Fig. 5. Reconstruction of total and spectral relative irradiance variations obtained by VIRGO for the year 1996. The employed solar model is able to fit both, total and spectral irradiance variations about equally well. In particular, the model reproduces the increase of spectral variability (RMS values) from longer (red channel) to shorter wavelength ranges (blue channel) of the spectrum. The fidelity of the shorter-term variations is partly limited by the restricted quality of the proxies and partly by the simplifications of the employed solar model.

Fig. 6. Observed (asterisk) and modelled (plus) irradiance variations during the passage of active region NOAA 7986 over the solar disk. The modelled curve is not able to reproduce the two peaks measured by VIRGO since the model does not take limb brightening effects into account.

the error at these channels below 1%. Unfortunately this cannot be achieved without simultaneously increasing the error in the blue channel well above 10%. The reason for this inconsistency between the total, red, green and the blue channel is currently not known.

Although, the model underestimates the variations in the blue somewhat, it is still able to reproduce the observed increase in spectral variability (RMS values) from longer to shorter wavelengths, i.e. from the red to the blue channel. Overall most of the peaks and dips are relatively well reproduced in all four spectral ranges. Both facular and spot contribution (restricted, however, mainly to the dip around day 330) are modelled about equally well.

Nevertheless on time-scales of days to weeks some deficits in the goodness of the temporal fidelity of the reconstructed
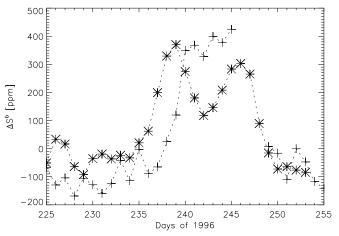
time series are present. For example, at the end of August 1996 (around day 240), the active region NOAA 7986 (dominated by faculae) passed the solar disk. Fig. 6 shows the observed (asterisk) and modelled (plus) irradiance variations for the blue channel during this period. The VIRGO observations clearly show two distinct peaks caused by limb brightening of the facular contrast (which is most strongly pronounced in the blue channel). The modelled irradiance variations, however, follow the Mg II core-to-wing ratio which being mainly of chromospheric origin does not exhibit a corresponding center-to-limb behaviour (Wehrli et al. 1997; cf. Lean et al. 1998). Hence the lack of fidelity of the reconstructed irradiance variations on time scales of days to weeks is partly due to the restricted quality of the used proxies and partly due to the simplifications of the model (namely the use of flux spectra).

By examining Fig. 7 one can see that all three colour channels of VIRGO are formed at about the same height, i.e. approximately between $z = -10$ and $+10$ km. The VIRGO data are therefore not able to distinguish between facular models having different temperature gradients, at least for a simple model such as ours, which neglects the center-to-limb variation of magnetic activity features. This is also confirmed by our reconstruction using facular model FAL-C2 which corresponds to a quiet Sun model with an effective temperature of T_{eff}=5870 K (see Table 2). Considering all four channels, both models (FAL-P2 and FAL-C2) reproduce the observations equally well.

However, the VIRGO data help to constrain the temperature of the radiation-forming layer of the facular model atmosphere. This temperature directly influences the appropriate faculae-to-spots filling factor ratio. If we restrict the range of faculae-to-spots filling factor ratios to values obtained from observations by Chapman et al. (1997), the facular temperature at the height responsible for the irradiance variations in the visible is constrained by the VIRGO data. We find a temperature enhancement of the faculae relative to the quiet Sun photosphere

Table 2. Comparison between modelled and observed RMS variations (in parts per million) for the four colour channels of VIRGO. Both models (FAL-P2 and FAL-C2) have a faculae-to-spots filling factor ratio of ≈ 20.

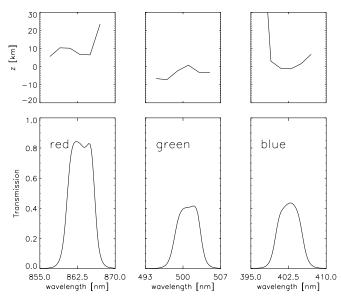|	σ_{tot}	σ_{red}	σ_{green}	σ_{blue}	
VIRGO	117.7	89.7	154.5	213.2	
Model (FAL-P2)	117.1 (-0.6%)	93.0 $(+3.7\%)$	156.8 $(+1.4\%)$	194.3 (-8.8%)	
Model (FAL-C2)	114.3 (-2.9%)	96.2 $(+7.2\%)$	155.5 $(+0.6\%)$	207.8 (-2.5%)	
	$\sigma_{red}/\sigma_{tot}$	$\sigma_{green}/\sigma_{tot}$	$\sigma_{blue}/\sigma_{tot}$	$\sigma_{red}/\sigma_{green}$	$\sigma_{green}/\sigma_{blue}$
VIRGO	0.76	1.31	1.81	0.58	0.73
Model (FAL-P2)	0.79 $(+4.3\%)$	1.34 $(+2.5\%)$	1.66 (-8.3%)	0.59 $(+2.2\%)$	0.81 $(+11.0\%)$
Model (FAL-C2)	0.84 $(+10.4\%)$	1.36 $(+3.6\%)$	1.82 $(+0.4\%)$	0.62 $(+6.6\%)$	0.75 $(+3.2\%)$

Fig. 7. Transmission functions and corresponding formation heights in the facular model for the three colour channels of VIRGO. Since all three channels are formed at about the same height they are not suited to distinguish between facular models of different temperature gradients.

of about $\Delta T = 100 \pm 20$ K at these levels, i.e. around $z = 0$–100 km. Both FAL-P2 and FAL-C2 satisfy this requirement.

5. Variability on the time-scale of the solar cycle

We now use our model to reconstruct solar spectral irradiance variations on time-scales of the solar cycle. Although no spectral irradiance measurements are available over such time-scales some predictions of our model can nevertheless be tested. Total irradiance variations measured during solar activity maximum and minimum as well as observations of changes in the faculae-to-spots filling factor ratio over the solar cycle can be compared to predictions of our model. This provides constraints on the effective temperature used for the spot and facular models.

In the following we consider the time-period between November 16, 1978 and December 31, 1996 covered by the composite TSI, i.e. from the maximum of solar cycle 21 to the

minimum between cycle 22 and cycle 23. The results are presented in Fig. 8. The solid curve represents the reconstructed irradiance while the observations are dotted. The predictions of the model are plotted only for the days on which A_s and R_{MG} as well as the irradiance value are available. Panel (a) shows the reconstruction over the whole period. The difference of 0.1% between minimum and maximum is well reproduced. The shorter-term variations plotted in panel (b) during high solar activity at the end of the considered period are also reasonably well reproduced. The RMS value of the reconstructed total irradiance over the whole period of time as well as for periods during the maximum and minimum phase separately, agree well with the observations and lie within an error smaller than 3%.

To reproduce the strong dips due to sunspot dimming during activity maximum the value of a_s has to be slightly increased compared to values inferred from the analysis for the VIRGO time period. This may be explained by a increasing contrast of sunspot versus photosphere with increasing sunspot area (Chapman et al. 1994, Steinegger et al. 1996) as well as by a possible decrease of the sunspot to photosphere intensity ratio from solar activity maximum to the following minimum (Albregtsen et al. 1983, Maltby et al. 1986). Both effects have not been accounted for in our model. Finally, the lack of center-to-limb variations of facular brightness may also contribute to this discrepancy.

The predicted faculae-to-spots filling factor ratio, averaged over the whole period of time, is about 13.5. To compare our findings directly to the observations made by Chapman et al. (1997) we follow their analysis and divide the time series into bins of 100 days and calculate the filling factor ratio for each bin separately. The results are plotted in Fig. 9. We separately evaluate the variations for the descending (days 1–2500 and 4000–6621) and the ascending (days 2500–4000) phase of solar cycles 21 and 22, respectively. The solid lines are linear fits to these three portions of the data. The dotted lines represent one sigma deviations arising from the scatter of the points around the regression lines. The filling factor ratio increases from about 16 during the maximum phase of cycle 21 to approximately 30 during the minimum between cycle 21 and 22. It then decreases to about 14 during the maximum of cycle 22 to finally increase again to approximately 24 at the minimum between cycle 22
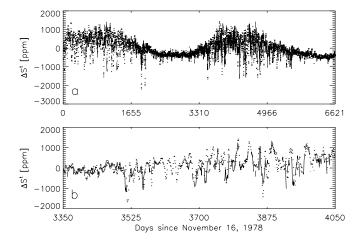
Fig. 8. Reconstruction (solid) of total solar irradiance composed by Fröhlich & Lean (1998). Long-term behavior, i.e. the difference between maximum and minimum (a) as well as shorter-term variations (b) are in general well reproduced.
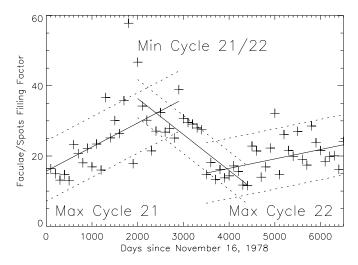

Fig. 9. The ratio of faculae-to-spots filling factors since November 1978 as predicted by our model. These results are in good agreement with the findings of Chapman et al. (1997) who derived faculae-to-spots filling factor ratios from observations. The solid lines are linear fits to the data for the descending and ascending phases of solar cycle 21 and 22, respectively. The dashed lines represent one sigma deviations (corresponding to the scatter of the crosses around the regression lines).

and 23. From the third regression line in Fig. 9 between days 3500 and 6621 (i.e. for the descending phase of cycle 22) we find: $\alpha_f/\alpha_s = 15.1 \pm 1.6 + (0.27 \pm 0.09) \cdot N/100$ where N is the number of days. This is in good agreement with the findings of Chapman et al. (1997) who derived for the same period of time: $\alpha_f/\alpha_s = 13.2 \pm 1.5 + (0.39 \pm 0.12) \cdot N/100$.

6. The UV spectral irradiance variations

To further test our model we consider the wavelength dependence of solar spectral irradiance variations between solar activity maximum and minimum. Such observations have been
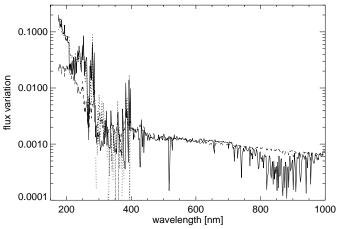

Fig. 10. Relative flux variations between solar activity minimum and maximum. Dotted line represents observed values according to Lean et al. (1997) and Lean (1991) while the solid line marks the reconstruction according to Solanki & Unruh (1998) based on the facular model FAL-P2 described in the text. Faculae-to-spots filling factor ratio at solar maximum is 12. The dashed line represents a reconstruction based on a different facular model (FAL-C2) which corresponds to a quiet Sun model with an increased effective temperature of T_{eff}=5870 K. The averaged faculae-to-spots filling factor ratio needs to be decreased to 10 in order to keep the variability over the solar cycle at 0.1%.

carried out mainly in the UV (Brueckner et al. 1993, London et al. 1993, Cebula et al. 1994 and Rottman et al. 1994). They are well suited to distinguish between facular models of different temperature gradients since the radiation between 174 nm and 300 nm (covered by our model) originates from different layers of the photosphere, i.e. is formed over a large height range of ≈ 50–400 km.

The spectrum of the relative irradiance variation between solar activity maximum and minimum produced by our model is plotted in Fig. 10 (solid line). The dotted line shows the observed ($\lambda < 400$ nm) irradiance variations according to Lean (1991) and Lean et al. (1997).

The filling factor of the spots, α_s, is chosen to correspond to the average observed value during activity maximum, while α_f is a free parameter determined by the fit to the observations. The best results are provided by an average faculae-to-spots filling factor ratio at activity maximum of 12 which accounts for a total variability of approximately 0.1% over the complete solar cycle and agrees well with the ratio observed at activity maximum by Chapman et al. (1997). The fit to the observations provided by the new model (FAL-P2 and spots with T_{eff}=5150 K) is of very nearly the same quality as that found by SU98. The changes to the thermal structures of the two model components described in Sect. 3 are driven not by the UV, but rather by the VIRGO and the composite TSI data.

In addition, we show a second reconstruction using facular model FAL-C2 which corresponds to a quiet Sun model with an increased effective temperature, of T_{eff}=5870 K (dashed). The faculae-to-spots filling factor ratio has been decreased to 10 in order to keep the total variability at the 0.1% level.

Both models provide relatively similar spectral irradiance variations between 350 nm and 700 nm. Only VIRGO's red colour channel is situated outside this spectral region, making it not so straightforward to distinguish between the models FAL-C2 and FAL-P2 by using the VIRGO data only (cf. Sect. 4). Only at wavelength shorter than 350 nm or longer than 700 nm do the models differ significantly. Hence, it is necessary to use UV or possibly infrared measurements to set tighter constraints on the temperature stratification of the facular model.

7. Stellar brightness variations

Our model allows us to calculate solar brightness variations within any prescribed spectral range between approximately 100 nm and 10^5 nm on time scales of weeks to the solar cycle. We can thus also predict the variability of the Sun in filter-bands used in stellar observations and hence enhance the accuracy of any comparison between solar and stellar brightness variations. Such an analysis is of particular interest in view of the results of Lockwood et al. (1992), who compared RMS brightness variations of the Sun with a sample of 33 Sun-like stars of weak to moderate chromospheric (magnetic) activity. Their measurements were carried out in two Strömgren filterbands centered on 472 nm ('b', blue) and 551 nm ('y', yellow), respectively, with 15–20 nm passband each (see dotted and dashed curves in Fig. 1). The Sun was found to exhibit significantly (2–3 times) lower brightness variations than its stellar counterparts showing a similar amount of Ca II H & K flux. This estimate is based on the assumption that the Sun radiates as a black body which implies that variations in the combination of Strömgren b- and y-bands exceed total irradiance variations by 20–25%. To check this assumption we calculate the solar RMS variation over a solar cycle in the b- and y-filterbands based on our results of Sect. 5 (we determine the RMS in the same manner as Lockwood et al. 1992).

The RMS variations in the b- and y-filterbands are about 25% and 15%, respectively, larger than in the total irradiance. If we recall that our model underestimates the enhancement in the blue, the b-band may actually show a 30% larger variation than the total irradiance. These values are in surprisingly good agreement with the estimate of Lockwood et al. based on a black body model. The difference in brightness of the Sun and Sun-like stars can hence not be attributed to an observational bias due to different wavelength ranges of the measurements. This conclusion is supported by the fact that the blue channel of VIRGO, which lies at an even smaller wavelength than Strömgren b, shows an RMS enhanced by only 60–80% compared to total irradiance — still well below the variability observed for Sun-like stars.

8. Summary and conclusions

We have tested the 3-component model of solar spectral irradiance variations presented by SU98 by comparing its predictions with both UV and visible spectral irradiance observations (the latter from VIRGO). Also, we have extended the model by using daily values of sunspot areas and Mg II core-to-wing ratio as proxies for the time variation of the sunspot and facular filling factor and provide improved estimates of the sunspot effective temperature and the average facular temperature stratification.

The model proves to be relatively successful in reproducing all total and spectral irradiance data sets. Thus it is able to simultaneously reproduce different aspects of the solar cycle, i.e. total irradiance (composite TSI/VIRGO), UV (Lean et al. 1997) and visible (VIRGO) spectral variations and changes of the faculae-to-spots filling factor ratio (Chapman et al., 1997). This confirms our assumption that the major part of solar irradiance variations (at least on time-scales of weeks to the solar cycle) are caused by magnetic fields at or close to the solar surface. To our knowledge no other model is capable of reproducing with similar accuracy as large a number and variety of irradiance and related data.

Careful comparison with the data, however, also reveal some of the limitations of the model. For example on the time scale of a solar rotation period the model prediction and the measured signal can differ significantly. Basically, there can be two causes for any discrepancy between the time dependence of calculated and observed irradiance. On the one hand it may be due to shortcomings in the proxies (data gaps, inaccurate measurements, or differences in the behaviour of proxy and the solar features it is to represent). Sunspot areas (in particular when used in conjunction with the sunspot positions) only suffer from the first two possible shortcomings, whereas facular proxies are subject to all three. The problem of the best facular proxy has been the subject of intense scrutiny (e.g. Brown & Evans 1980, Foukal & Lean 1988, Foukal 1993, Pap et al. 1994, Fligge & Solanki 1998, Lean et al. 1998). We do not intend to contribute to that debate. It is sufficient to point out that at the times when the model differed most significantly from the data the facular proxy in general already showed a behaviour incompatible with the observations. This implies that a fair portion of the discrepancy is caused by the facular proxy. The problem is mainly the difference between the center-to-limb variation of photospheric faculae and the Mg II core-to-wing ratio. The faculae show an increase in contrast from the center of the solar disc to its limb, whereas the Mg II core-to-wing ratio shows no such increase (as is to be expected for almost any proxy of chromospheric origin).

The center-to-limb variation of the facular contrast is, however, not just a problem of the proxy. By using flux spectra to describe the irradiance contributions of the different solar features we preclude it elsewhere in the model as well. Comparison with the data suggests that this is the simplification leading to the largest errors.

Note that the introduction of a center-to-limb variability could well influence the temperature stratification of the facular model which provides the best fit to the observations.

Other assumptions may also be responsible, however, for a part of the discrepancy. One is the assumption that lines are formed at the same height in faculae and quiet Sun which underlies our simple way of determining the facular spectrum. Another is the assumption that all faculae and spots have the same thermal structure. Finally, even our basic assumption that irradiance variations are caused by solar surface magnetism may

be responsible for a part of the remaining discrepancy. Each of these will need careful consideration in a later analysis.

References

Albregtsen F., Joras P.B., Maltby P., 1983, Solar Phys. 90, 17

Brasseur G., Solomon S., 1984, *Aeronomy of the Middle Atmosphere*, D. Reidel, Hingham, Mass.

Brown G.M., Evans D.R., 1980, Solar Phys. 66, 233

Brueckner G.E., Edlow K.L., Floyd L.E., Van Hoosier M.E., 1993, J. Geophys. Res. 98, 10695

Cebula R.P., Hilsenrath E., Deland M.T., 1994, in The Sun as a Variable Star: Solar and Stellar Irradiance Variations, J. Pap, C. Fröhlich, H.S. Hudson, S.K. Solanki (Eds.), Cambridge University Press, Cambridge, IAU Coll. 143, 81

Chapman G.A., Cookson A.M., Dobias J.J., 1994, Astrophys. J. 432, 403

Chapman G.A., Cookson A.M., Dobias J.J., 1997, Astrophys. J. 482, 541

Del Toro Iniesta J.C., Tarbell T.D., Ruiz Cobo B., 1994, Astrophys. J. 436, 400

Donnelly R.F., White O.R., Livingston W.C., 1994, in The Sun as a Variable Star: Solar and Stellar Irradiance Variations, J. Pap, C. Fröhlich, H.S. Hudson, S.K. Solanki (Eds.), Cambridge University Press, Cambridge, IAU Coll. 143, 69solar Ca II K index and the Mg II core-to-wing ratio

Fligge M., Solanki S.K., 1998, Astron. Astrophys. , in press

Fontenla J.M., Avrett E.H., Loeser R., 1993, Astrophys. J. 406, 319

Foukal P., 1993, Solar Phys. 148, 219

Foukal P., Lean J., 1988, Astrophys. J. 1988, 347

Fröhlich C., Lean J., 1998, in New Eyes to see inside the Sun and Stars, F.L. Deubner (Ed.), Kluwer Academic Publ., Dordrecht, Netherland, IAU Symp. 185 in press

Fröhlich C., Pap J.M., Hudson H.S., 1994, Solar Phys. 152, 111

Fröhlich C., Romero H., Roth H. et al., 1995, Solar Phys. 162, 101

Fröhlich C., Crommelynck D.A., Wehrli C. et al., 1997, Solar Phys. 175, 267

Haigh J.D., 1994, Nature 370, 544

Haigh J.D., 1996, Science 272, 981

Heath D.F., Schlesinger, B.M., 1986, J. Geophys. Res. 91, 908

Hudson H.S., Silva S., Woodard M., Willson R.C., 1982, Solar Phys. 76, 211

Kurucz R.L., 1991, in Stellar Atmospheres: Beyond Classical Models, L. Crivellari, I. Hubeny, D.G. Hummer (Eds), Kluwer, Dordrecht, p. 441

Kyle H.L., Hoyt D.V., Hickey J.R., 1994, Solar Phys. 152 9

Lean J., 1988, Adv. Space Res., 8, 263

Lean J., 1991, Reviews of Geophysics 29, 505

Lean J., Rottman G.J., Kyle H.L., Woods T.N., Hickey J.R., Puga L.C., 1997, J. Geophys. Res. 1997, submitted

Lean J.L., Cook J., Marquette W., Johannesson A., 1998, Astrophys. J. 492, 390

Lockwood G.W., Skiff B.A., Baliunas S.L., Radick R.R., 1992, Nature 360, 653

London J., Rottman G.J., Woods T.N., Wu F., 1993, Geophys. Res. Lett. 20, 1315

Maltby P., Avrett E.H., Carlsson M. et al., 1986, Astrophys. J. 306, 284

Pap J.M., 1992, Astron. Astrophys. 264, 249

Pap J.M., Willson R.C., Fröhlich C., Donelly R.F., Puga L., 1994, Solar Phys. 152, 13

Rees M.H., 1989, Physics and Chemistry of the upper atmosphere, Cambridge University Press, New York

Rottman G.J., Woods T.N., White O.R., London J., 1994, in The Sun as a Variable Star: Solar and Stellar Irradiance Variations, J. Pap, C. Fröhlich, H.S. Hudson, S.K. Solanki (Eds.), Cambridge University Press, Cambridge, IAU Coll. 143, 73Irradiance Observations from the UARS/SOLSTICE Experiment.

Severino G., Gomez M.T., Caccin B., 1994, in Solar Surface Magnetism, R.J. Rutten, C.J. Schrijver (Eds), Kluwer, Dordrecht, p. 169

Solanki S.K., Unruh Y.C., 1998, Astron. Astrophys. 329, 747

Steinegger M., Brandt P.N., Pap J., Schmidt W., 1990, Solar Phys. 170, 127

Steinegger M., Brandt P.N., Haupt H.F., 1996, Astron. Astrophys. 310, 635

Wehrli C., Fröhlich C., Anklin M. et al., 1997, in Correlated phenomena at the Sun, in the heliosphere and in geospace, B. Fleck, A. Wilson (Eds.), 31. ESLAB Symposium, ESA SP-415, Noordwjick, NL, in press

Willson R.C., Hudson H.S., 1988, Nature 332, 810

Willson R.C., Hudson H.S., 1991, Nature 351, 42